Trapping of rare earth-doped nanorods using quasi Bessel beam optical fiber tweezers

R. A Minz, U. Tiwari, A. Kumar, S. Nic Chormaic, K. Lahlil, T. Gacoin, S. K Mondal, J. Fick

Research Article | Vol. 4, No. 2 / 15 February 2021 / OSA Continuum 364

Trapping of rare earth-doped nanorods using quasi Bessel beam optical fiber tweezers

R. A. Minz,[1,2,3,6] U. Tiwari,[1,3,6] A. Kumar,[1] S. Nic Chormaic,[1,4] K. Lahlil,[5] T. Gacoin,[5] S. K. Mondal,[3] and J. Fick[1,*]

[1] *Université Grenoble Alpes, CNRS, Institut Néel, 38000 Grenoble, France*
[2] *Academy of Scientific and Innovative Research, CSIR-CSIO, 160030, India*
[3] *Central Scientific Instruments Organisation, Chandigarh 160030, India*
[4] *Light-Matter Interactions for Quantum Technologies Unit, Okinawa Institute of Science and Technology Graduate University, Onna, Okinawa 904-0495, Japan*
[5] *Laboratoire de Physique de la Matière Condensée, École Polytechnique, CNRS, Université Paris Saclay, 91128 Palaiseau, France*
[6] *These authors contributed equally to the work*
[*] *jochen.fick@neel.cnrs.fr*

Abstract: We demonstrate optical trapping of rare earth-doped $NaYF_4$:Er/Yb nanorods of high aspect ratio (length 1.47 μm and diameter 140 nm) using a quasi Bessel beam (QBB) generated by positive axicon optical fiber tips. Propulsion or trapping of the nanorods is demonstrated using either single or dual fiber nano-tip geometries. The optical force exerted on the trapped nanorods, their velocities, and their positions have been analyzed. We determine the trap stiffness for a single nanorod to be 0.12 pN/μm (0.003 pN/μm) by power spectrum analysis and 0.13 pN/μm (0.015 pN/μm) by Boltzmann statistics in the direction perpendicular to (along) the fiber axes for an average optical power of 34 mW. The experiments illustrate the advantage of using a QBB for multiple nanorod trapping over a large distance of up to 30 μm.

1. Introduction

Since their earliest demonstrations [1], optical tweezers have found many applications in physics, biology, chemistry and medical research; a very comprehensive review of the field is contained in [2]. There have been numerous research efforts to optically manipulate particles of different shapes, sizes, materials, and even using different optical arrangements [3–6] compared to the original configuration that used a high numerical aperture (NA) lens to create a single beam, gradient trap. Due to their small footprint, ease of alignment, and integration with existing optical setups, trapping experiments with optical fibers are one specific platform that has seen strong progress in recent years. Different fiber configurations have been developed including tapered optical fibers [7–12], structured optical fibers [13–15], single fibre tips [16,17], tapered fiber tips [18–22], and lensed fiber tips [23,24].

Considering the wide application of rare earth elements in bioimaging, biosensing, and therapeutics, trapping rare earth-doped nanoparticles is of particular interest. For example, $NaYF_4$:Er/Yb nanorods, due to their up-conversion fluorescence emissions, are potential candidates for realizing single photon sources, bio-imaging, or in single-molecule spectroscopy [25,26]. However, three-dimensional manipulation and motion control of such particles is key to many of the potential applications. In 2018, Leménager et al. [27] demonstrated trapping of such co-doped $NaYF_4$ nanorods using a single and dual fiber tip optical tweezers and, more recently, europium-doped $NaYF_4$ nanorods (of average length 1.2 μm and diameter 120 nm) have been trapped using a single fiber tip optical tweezers [22] for an orientation-resolved spectroscopic study on the nanorod's photoluminescence. This work also indicates the challenges in using

#417151 https://doi.org/10.1364/OSAC.417151
Journal © 2021 Received 10 Dec 2020; revised 8 Jan 2021; accepted 11 Jan 2021; published 25 Jan 2021

OSA CONTINUUM

tapered fiber tips, as the particles were attracted toward the tip and trapped in contact with it, rendering a study on the photoluminescence polarization through the fiber impossible.

While optical fiber tip trapping generally relies on Gaussian beam profiles, recent works indicate that non-Gaussian beams also hold promise for efficient particle trapping [28–30]. One type of non-Gaussian beam that can be considered is the quasi Bessel beam (QBB). It can be exploited for three-dimensional trapping of particles that have a high aspect ratio and asymmetry due to the large depth-of-focus offered [31,32]. The challenge lies in designing optical elements that can efficiently generate QBBs with the desired optical properties for trapping. Different approaches can be used [30,32,33] and a modified optical fiber tip [30,34] has proven to convert a Gaussian beam into a QBB with very low divergence and a very small spot size, while being very easily integrated into experimental setups. Such fibre-based QBBs have already been used for micro- and nanoparticle trapping [28,35].

In this work, we demonstrate optical trapping of $NaYF_4$:Er/Yb single and multiple nanorods with a high aspect ratio using a customized dual tip optical fiber tweezers setup. A Gaussian beam is converted into a QBB via a positive axicon structure on the fiber nano-tip [34]. The properties of the optical trap are studied by applying the power spectrum analysis (PSA) [36,37] or the Boltzmann statistics method to the particle position fluctuations [38].

2. Experimental details

2.1. Optical fiber tips for quasi Bessel beam generation

Although Bessel beams can be generated using free-space optics [31], this can add bulkiness and alignment issues to the design of optical tweezers. An alternative approach to generate QBBs is to structure the tip of an optical fiber; the fiber can then be used for optical trapping [28,35]. For the work reported herein, we fabricate an axicon by chemical wet-etching of highly germanium-doped optical fibers (StokerYale PS-1550-Y3 with a N.A. of 0.17, mode field diameter of 7 μm and cladding diameter of 125 μm) [39], see [34] for details. The etching and tip shape are determined by surface tension, capillary action, and the different etching rates for the fiber core and cladding materials. A simple etching mechanism is used; the fiber is vertically aligned and dipped for 40 minutes inside a polymer coated tube containing 48% hydrofluoric acid with an elevated meniscus. The meniscus defines the shape of the fiber axicon tip, guided by capillary action [34,40].

Figure 1(a) is a scanning electron microscope (SEM) image of a typical axicon tip. The fiber axicon emission properties are studied by mapping the transverse (perpendicular to the fiber axis, that is along x or y, we generally use the y-direction) and longitudinal (along the fiber axis, z) beam profiles. The quality of the fabricated tips—thence their suitability for trapping experiments—is determined from these beam profiles. In Fig. 1(b), the propagation characteristics of the longitudinal beam profile from a sample axicon tip are shown for laser light at 808 nm propagating in the fiber. The longitudinal beam profile measurements were taken by collecting the light from the positive axicon tip using a 50× microscope objective coupled to a CMOS camera. The objective was fixed in place, whereas the axicon tip was moved towards it, and therefore also towards the camera, for a distance of 0.02 mm. The emission profile reveals the quasi Bessel like properties of the beam. In particular, we observe that the central spot of the beam is reasonably non-diffracting over the short distance of 0.02 mm considered. The inset shows the beam profile when directed onto a screen, with the image captured by a CMOS camera.

For particle trapping experiments, we use two fibers, each having a positive axicon on its end, in a tip-to-tip configuration. Before conducting the trapping experiments, we first determine the optimum fiber tip-to-tip separation that yields the smallest beam waist. This yields the highest field intensity, or, in other words, the optimum tip-to-tip separation for stable trapping. With this in mind, we first measure the transmission profile in air. Laser light of wavelength 808 nm is coupled into the pigtail of one of the optical fibers (the source probe) and the transmitted

OSA CONTINUUM

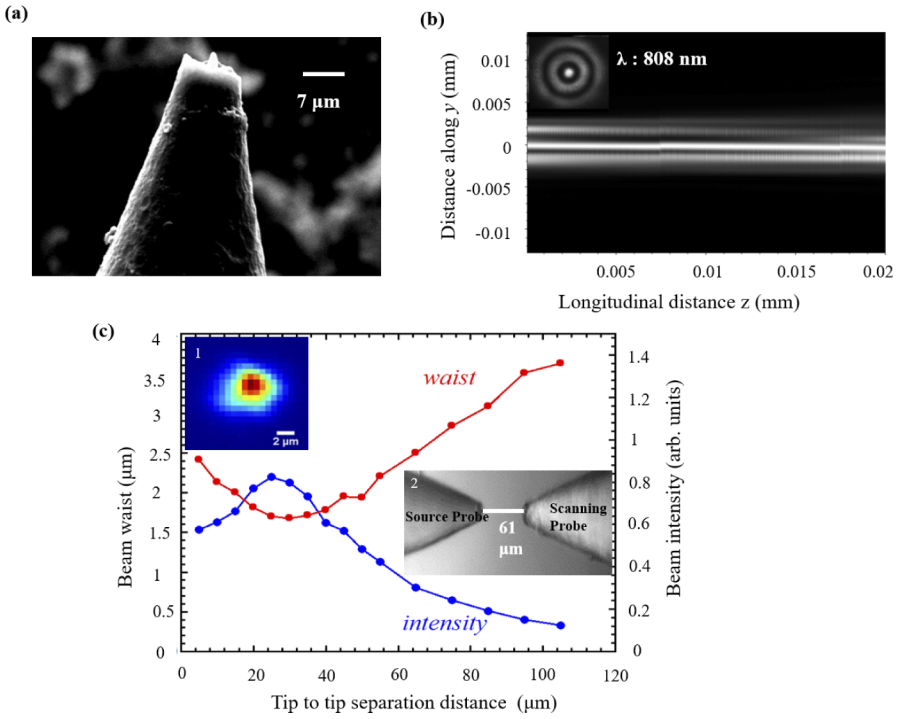

Fig. 1. (a) SEM image of a positive axicon optical fiber tip. (b) Longitudinal emission profile from a positive axicon tip in air. The *y*-axis is a transverse direction. The '0' point along the longitudinal direction indicates the initial separation between the fibre tip and the objective. Inset: Quasi Bessel beam profile for 808 nm light. (c) Average beam waist and intensity as a function of fiber tip-to-tip separation in water. Inset 1: A typical transverse-plane intensity map for 808 nm light at the waist region for a tip-to-tip distance of 24.69 μm. Inset 2: Two positive axicons with in a tip-to-tip configuration with a separation of 61 μm as used for transverse mapping and trapping experiments.

light is collected by scanning the position of the second optical fiber (the scanning probe) in the transverse (*xy*) plane to generate a map of the beam profile. The beam is directed onto a screen and the image is captured by a CMOS camera. Next, the beam parameters are measured by inserting the fiber tips into deionized water since this mimics the actual trapping environment. Figure 1(c) is a plot of the average measured beam waist and intensity for the transverse directions as a function of the tip-to-tip separation when light of 808 nm propagates in the fiber. The beam waist has a minimum value of ~ 1.64 μm at a tip-to-tip distance of 24.7 μm – beyond this distance, the waist increases as the distance between the tips increases and the emission angle is around 2°. This is about 4 times smaller than for tapered fiber tip optical traps [19]. Inset 1 in Fig. 1(c) is a typical transverse beam profile obtained for a tip-to-tip separation of 24.7 μm, while the tip-to-tip fiber configuration is shown in Inset 2.

2.2. Fiber-based optical tweezers setup

A schematic of the fiber-based optical tweezers setup is given in Fig. 2. The trapping laser beam at 808 nm, provided from a diode laser (Lumics LU0808M250), is split into two paths via a 50:50 polarizing beam splitter. Each fiber tweezers tip is mounted on an *xyz* piezoelectric translation stage for alignment purposes. A droplet of deionized water solution containing the nanorods is placed in a custom-designed fluid chamber, see inset to Fig. 2, which consists of an O-ring sealed

OSA CONTINUUM

with vacuum grease and placed between two glass slides. The O-ring has two slits for inserting the fiber tips. An optical microscope consisting of a 50× objective with a long working distance (13.9 mm) combined with a CMOS camera (Hamamatsu, ORCA FLASH 4.0 LT) is used for particle imaging. Particle trapping videos are recorded at a frame rate of 200 f/sec and with a resolution of 96 nm/pixel. A particle tracking algorithm has been developed in the open source Scilab environment and is used to extract the time-dependent particle positions from the trapping videos. This algorithm is based on numerical fitting of a two-dimensional Gaussian function to the particle image of each video frame. The light powers in the following are all measured at the output of the fibre tip(s).

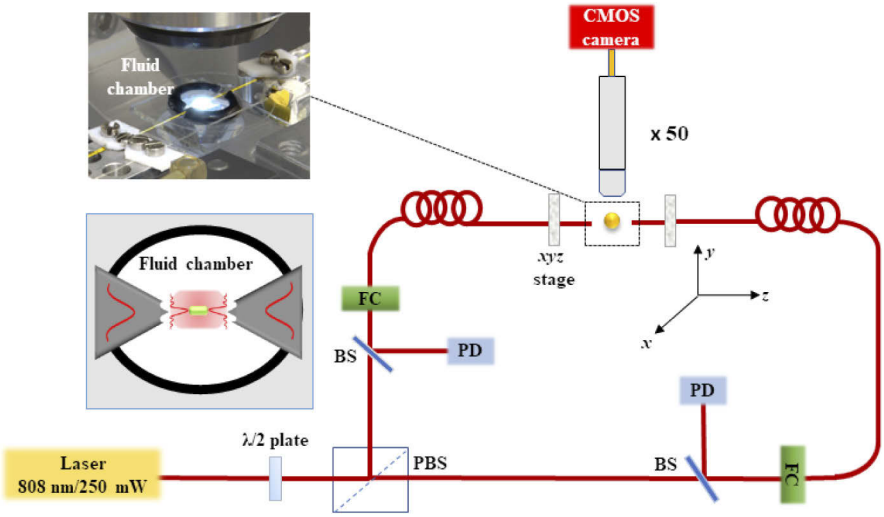

Fig. 2. Schematic of the fiber-based optical tweezers setup. PD: photodiode, BS: beam splitter, PBS: polarizing BS, FC: fiber coupler. Inset: Image of the fluid chamber that is placed at the trapping region between the fiber tips.

2.3. Nanorod preparation and characterization

The $NaYF_4$:Er/Yb nanorods were prepared by 45 mM (1.8 g) of NaOH in 6 ml of water mixed with 15 ml of ethanol (EtOH) and 30 ml of oleic acid (OA) under stirring. The following were added to the mixture: 273 mg of $Y(Cl)_3$, 10.1 mg of YbCl, 6.7 mg of $ErCl_3$ and 378 mg of NH_4F dissolved in 4 ml of water. The solution was then transferred to a 75 ml autoclave and heated at 190°C for 24 hrs under stirring. After cooling down to the ambient temperature, the resulting nanoparticles were precipitated by the addition of 50 ml of ethanol, collected by centrifugation, then washed with water and ethanol several times. They were finally dried under vacuum and kept as a white powder. A scanning electron microscope (SEM) image of the prepared nanorods is given in Fig. 3, along with their length and diameter distribution.

For the trapping experiments, fonctionalization by ligand exchange is needed to ensure good dispersion in water. Hence 20 mg of $NaYF_4$ in oleic acid NPs are sonicated and centrifuged three times with 2 ml aqueous citrate solution (0.2 M), then washed with EtOH and water to remove the remaining oleic acid molecules; finally the nanorods are well dispersed in water [41–43]. Nanorods used in the trapping experiments reported herein have an average diameter of ~140 nm and a length of ~1.47 μm. For the trapping experiments, the nanorods were diluted in deionized water at a ratio of 1:2 and injected in the fluid chamber as discussed in Section 2.2.

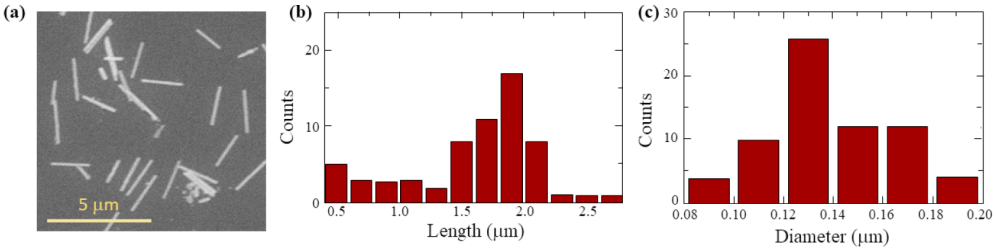

Fig. 3. (a) SEM image of the $NaYF_4$:Er/Yb nanorods. (b) Length and (c) diameter distribution of the nanorods.

3. Optical trapping experiment

3.1. Nanorod manipulation using a single fiber axicon tip

We first studied the nanorod behavior using a single axicon tip to see if they can be stably trapped. We observed that the nanorods are attracted toward the center of the beam via the gradient force, while simultaneously being repelled from the fiber tip itself. Aside from the fact that the beam is non-Gaussian, there are several features that could lead to this behavior, see Fig. 1(c): (i) the beam is initially converging and later diverging, so particles are not attracted to the fiber tip compared to in earlier work [22] and (ii) the emission angle is quite low at 2°, hence the gradient force is also low compared to that for tapered fiber tips [19]. Previous work by Leménager et al. [21] showed that stable nanorod trapping is influenced by the length of the nanorods when using dual or single tapered fiber tips with Gaussian beam transmission profiles. However, we clearly observe that nanorods cannot be trapped using a single axicon fiber tip, but rather are pushed away from it.

Figure 4 is a plot of the trajectory of three distinct nanorods as they are pushed away from the fiber tip at an output power of 45.3 mW. The force acting on the particle in the transverse direction is small compared to that in the longitudinal (z-) direction. The overall force varies by about a factor of 4 with distance due to the variation in the quality of the QBB from the source axicon. The force on the particle is also calculated using the Langevin equation of motion [44] as the particle is pushed away from the fiber and this is also plotted in Fig. 4 via the color scale bar. Hence, using a single fiber tip, nanorod manipulation is indeed possible at a distance of some micron from the fiber tip with a power of 45.3 mW; however, we see no clear evidence of trapping.

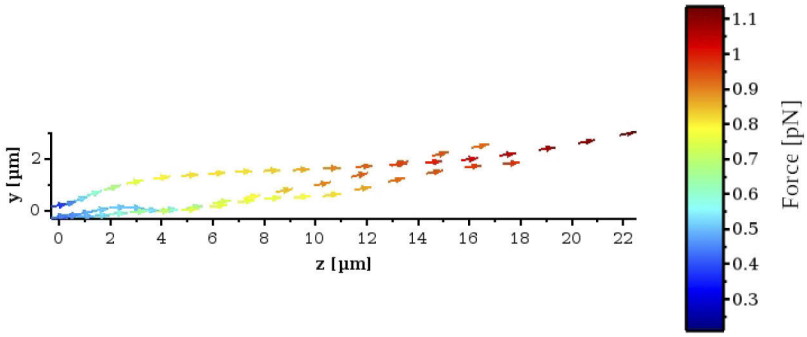

Fig. 4. Trajectory of three distinct nanorods as they are pushed away from a single fiber tip axicon positioned at (0,0) in the yz plane. The color bar represents the calculated force at each position of the nanorod where the maximum force applied on the nanorod is about 1.1 pN at 22 μm away from the axicon tip. The power at the output of the fibre is 45.3 mW.

OSA CONTINUUM

3.2. Nanorod trapping using two fiber axicon tips

Next, we studied trapping of nanorods by placing the prepared particle sample between two fiber axicon tips. For the typical trapping experiments reported here, the maximum optical power measured at the two fiber tips is ~26.5 mW and ~41.5 mW. The imbalance in powers is assumed to arise from the fact that the tips are not identical because of the fabrication process. In the following, we give the average of the two powers for simplicity unless otherwise stated.

Both single and multiple nanorods were trapped using this configuration, see images in Figs. 5(a) and 5(b). Figure 5(a) is a bright field image of a single trapped nanorod. The Er/Yb-doped nanorods are efficiently pumped by the 808 nm trapping laser, allowing us to record fluorescence images. In Fig. 5(b), we present a fluorescence image of three trapped nanorods. The transverse displacement of the trapped nanorods relative to each other is also evident and in future work we would aim to study this in more detail. Using the aforementioned particle tracking algorithm, the trajectory of a particle in the yz plane during a given time interval can be plotted, see Fig. 5(c) for a typical trajectory followed by a single trapped nanorod. Figure 5(d) is the time series of the particle position along the directions longitudinal and transverse with respect to the fiber axis.

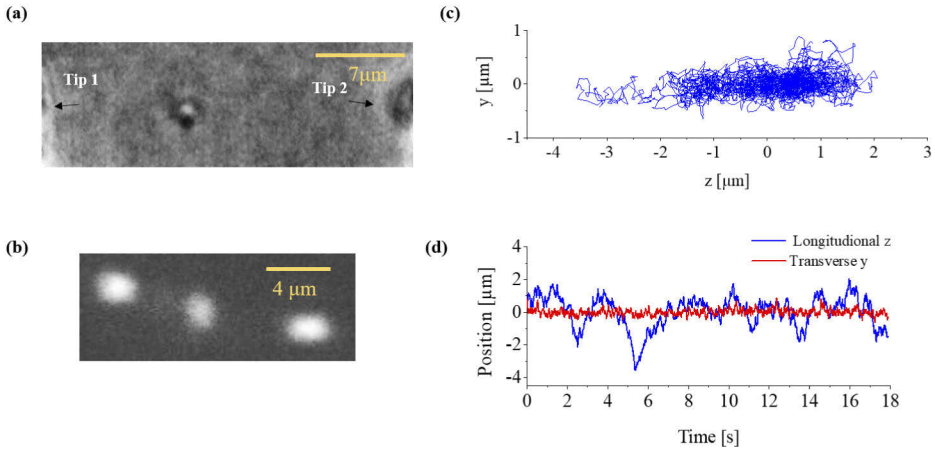

Fig. 5. (a) Image of a singled trapped nanorod with an average power of ~34 mW at the fibre outputs. (b) Fluorescence image of multiple trapped nanorods with an average light power of ~28.4 mW at the fibre outputs. (c) Particle trajectory for the single trapped nanorod in (a). (d) Time series of the particle position along the transverse (blue curve) and longitudinal (red curve) directions at 200 frames/second with an image resolution of 97nm/pixel.

4. Results and discussion

To determine the trapping efficiency, we have calculated the trap stiffness for a trapped particle at different powers using Boltzmann statistics (BS) and power spectrum analysis (PSA). The trap stiffness coefficient, κ, of an optical trap defines the relation between the exerted force magnitude, F, and the displacement, x, of the particle with respect to the trap center, i.e., $\kappa = -F/x$. For calculating the stiffness of the trap, the most reliable and fastest method is based upon PSA [36,37], where the power spectrum is fitted to a Lorentzian function as follows

$$P(f_k) = \frac{k_B T}{2\pi^2 \gamma_0 (f_c^2 + f_k^2)}, \tag{1}$$

OSA CONTINUUM

where γ_0 is the Stokes' coefficient for friction, k_B is the Boltzmann constant, and T is the temperature. Considering the geometry of the nanorods, we use a corrected expression for $\gamma_0 = (4\pi l\eta)/(\ln(l/d) + 0.84)$, where η, l, and d are the dynamic viscosity of the host medium, the nanorod length, and diameter, respectively. We use the following values: $\eta(300K) = 0.865$ mPa·s for water, $l = 1.47$ μm, and $d = 140$ nm. The 0.84 term is an end-effect correction valid for the range of l/d for the nanorods used herein [45]. The corner frequency, f_c, is related to the trap stiffness constant through $f_c = \kappa/2\pi\gamma_0$. In Fig. 6(a), a typical power spectrum for trapped nanorods at an average optical power of 34 mW is plotted. The corresponding trap stiffnesses are 0.122 pN/μm and 0.003 pN/μm in the transverse and longitudinal directions, respectively.

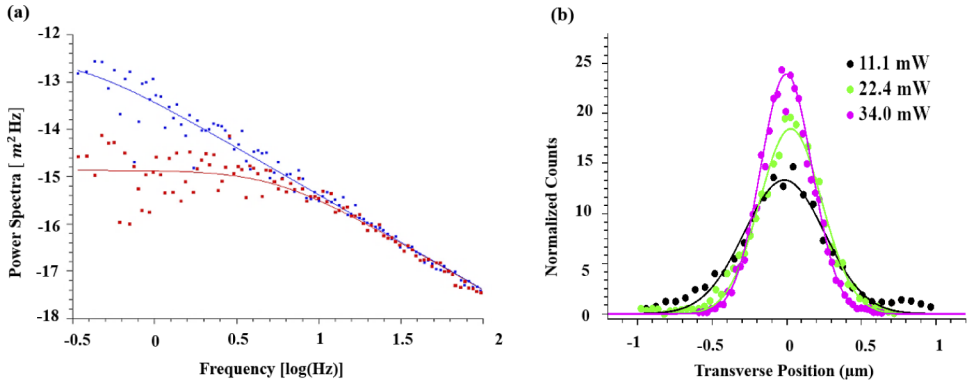

Fig. 6. (a) Power spectra for the transverse (red) and longitudinal (blue) position of a trapped nanorod at 30 μm tip-to-tip distance(b) Boltzmann distribution of the trapped particles for different powers as measured in the transverse direction at 30 μm tip-to-tip distance.

An alternative approach to analyze the trap behavior is to use Boltzmann statistics [38]. Here, the position probability density function, $P(x)$, is used to determine the trapping potential, $U(x)$, from [35]

$$P(x) = \frac{1}{Z} e^{\frac{-U(x)}{k_B T}}, \tag{2}$$

where Z is the partition function. For a harmonic trapping potential with $U(x) = \kappa x^2/2$, the trap stiffness coefficient, κ, is directly obtained by fitting the probability density function to a Gaussian function $P(x) = \exp(\kappa x^2/2k_B T)$. Hence, we determine trap stiffnesses of 0.130 pN/μm and 0.015 pN/μm for the transverse and longitudinal directions, respectively, at an average power of 34 mW, see Fig. 6(b).

Once a nanorod is trapped in the equilibrium position between the two fiber tips, trapping videos are recorded at different laser powers from 11 mW to 34 mW. The trapped particle position fluctuations are analyzed and the associated trap stiffnesses are calculated for both the transverse and longitudinal directions as plotted in Fig. 7. We find reasonable agreement between the values obtained using the two different methods. The transverse power-normalized trap stiffnesses, $\tilde{\kappa}_{trans.}$, are 4.4 fN/μm/mW and 3.9 fN/μm/mW for BS and PSA, respectively. In the longitudinal direction the difference between the two methods is more important (0.6 fN/μm/mW and 0.2 fN/μm/mW), mainly because of the low absolute values, near the experimental resolution. These values are determined from the slopes of the plots in Fig. 7.

The trapping efficiency is more than nine times higher in the transverse direction than in the longitudinal direction. A similarly high ratio was already observed in trapping experiments with similar fibers but using 1 μm polystyrene spheres [35]. It is related to the low dispersion of the QBB of only 2°. Using tapered fiber tips with a four times larger emission angle of about 8°, results in higher longitudinal trapping efficiencies and a ratio of about three [19]. In general the

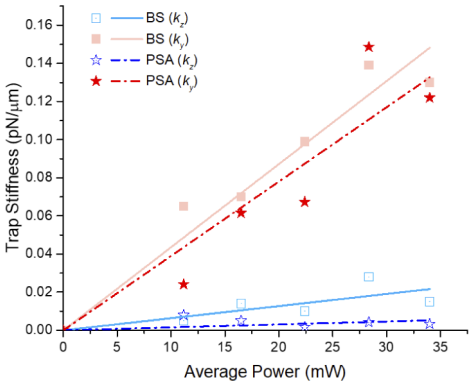

Fig. 7. Trap stiffness of the trapped nanorods along the transverse (upper plots, red shades) and longitudinal (lower plots, blue shades) directions as a function of the average trap power calculated using PSA (stars) and BS (squares) methods. The lines represent linear fits to the data.

trapping efficiency is high enough for maintaining the nanorods inside the trapping volume. The transverse efficiency is about 20 times lower than for 1 μm spheres, but one has to consider the 23 times lower volume of the nanorod.

5. Conclusion

In conclusion, we have experimentally demonstrated that a dual beam optical fiber tip tweezers generating quasi Bessel beams with a minimum beam waist of 1.64 μm at 24.7 μm tip-to-tip distance can be used to trap asymmetric nanorods at different optical powers. Nanorods of rare earth-doped $NaYF_4$:Er/Yb with an average length of 1.47 μm and diameter of 140 nm have been successfully trapped. Although the trap stiffness coefficients are low compared to other dual fiber tip tweezers for nanoparticles (see, for example, [21]), the quasi Bessel beam allows for a relatively large separation between the tips, thereby enabling long-range trapping of nanorods using a configuration similar to that for long-range microparticle trapping [35]. This is particularly useful for exploring chains of trapped particles, optical binding effects over longer distances, and for integration of the fiber tips into existing optical tweezers setups for spectroscopic studies.

Funding. Council of Scientific and Industrial Research, India (Raman Fellowship); CEFIPRA (Raman Charpak Fellowship); Agence Nationale de la Recherche (ANR-16-CE24-0014-01).

Disclosures. The authors declare no conflicts of interest.

References

1. A. Ashkin, J. M. Dziedzic, J. E. Bjorkholm, and S. Chu, "Observation of a single-beam gradient force optical trap for dielectric particles," Opt. Lett. **11**(5), 288–290 (1986).
2. J. Gieseler, J. R. Gomez-Solano, A. Magazzù, I. P. Castillo, L. P. García, M. Gironella-Torrent, X. Viader-Godoy, F. Ritort, G. Pesce, A. V. Arzola, K. Volke-Sepulveda, and G. Volpe, "Optical tweezers: A comprehensive tutorial from calibration to applications," DOI:10.1364/AOP.394888 (2020).
3. N. K. Paul and B. A. Kemp, "Optical manipulation of small particles on the surface of a material," J. Opt. **18**(8), 085402 (2016).
4. X. Han, V. G. Truong, P. S. Thomas, and S. Nic Chormaic, "Sequential trapping of single nanoparticles using a gold plasmonic nanohole array," Photonics Res. **6**(10), 981–986 (2018).
5. F. Kalantarifard, P. Elahi, G. Makey, O. M. Maragò, F. Ömer Ilday, and G. Volpe, "Intracavity optical trapping of microscopic particles in a ring-cavity fiber laser," Nat. Commun. **10**(1), 2683 (2019).
6. A. L. Ravindranath, M. S. Shariatdoust, S. Mathew, and R. Gordon, "Colloidal lithography double-nanohole optical trapping of nanoparticles and proteins," Opt. Express **27**(11), 16184–16194 (2019).

OSA CONTINUUM

7. G. Brambilla, G. Senthil Murugan, J. S. Wilkinson, and D. J. Richardson, "Optical manipulation of microspheres along a subwavelength optical wire," Opt. Lett. **32**(20), 3041–3043 (2007).
8. H. Lei, Y. Zhang, X. Li, and B. Li, "Photophoretic assembly and migration of dielectric particles and Escherichia coli in liquids using a subwavelength diameter optical fiber," Lab Chip **11**(13), 2241–2246 (2011).
9. S. Skelton, M. Sergides, R. Patel, E. Karczewska, O. Maragó, and P. Jones, "Evanescent wave optical trapping and transport of micro and nanoparticles on tapered optical fibers," J. Quant. Spectrosc. Radiat. Transfer **113**(18), 2512–2520 (2012).
10. I. Gusachenko, V. Truong, M. Frawley, and S. Nic Chormaic, "Optical nanofiber integrated into optical tweezers for in situ fiber probing and optical binding studies," Photonics **2**(3), 795–807 (2015).
11. A. Maimaiti, D. Holzmann, V. Truong, H. Ritsch, and S. Nic Chormaic, "Nonlinear force dependence on optically bound micro-particle arrays in the evanescent fields of fundamental and higher order microfibre modes," Sci. Rep. **6**(1), 30131 (2016).
12. G. Tkachenko, I. Toftul, C. Esporlas, A. Maimaiti, F. L. Kien, V. G. Truong, and S. Nic Chormaic, "Light-induced rotation of dielectric microparticles around an optical nanofiber," Optica **7**(1), 59–62 (2020).
13. M. Daly, V. G. Truong, and S. Nic Chormaic, "Evanescent field trapping of nanoparticles using nanostructured ultrathin optical fibers," Opt. Express **24**(13), 14470–14482 (2016).
14. X. Ni, M. Wang, R. Wang, Y. Huang, Y. Wang, and D. Guo, "Optical manipulation of microparticles with a fiber tip containing a hollow cavity," Opt. Quantum Electron. **50**(6), 238 (2018).
15. Y. Yu, T.-H. Xiao, Y.-X. Li, Q.-G. Zeng, B.-Q. Li, and Z.-Y. Li, "Tunable optical assembly of subwavelength particles by a microfiber cavity," Nanotechnology **30**(25), 255201 (2019).
16. A. Constable, J. Kim, J. Mervis, F. Zarinetchi, and M. Prentiss, "Demonstration of a fiber-optical light-force trap," Opt. Lett. **18**(21), 1867–1869 (1993).
17. J. Chen, Z. Kang, S. K. Kong, and H.-P. Ho, "Plasmonic random nanostructures on fiber tip for trapping live cells and colloidal particles," Opt. Lett. **40**(17), 3926–3929 (2015).
18. Z. Liu, C. Guo, J. Yang, and L. Yuan, "Tapered fiber optical tweezers for microscopic particle trapping: fabrication and application," Opt. Express **14**(25), 12510–12516 (2006).
19. J.-B. Decombe, S. Huant, and J. Fick, "Single and dual fiber nano-tip optical tweezers: trapping and analysis," Opt. Express **21**(25), 30521–30531 (2013).
20. J.-B. Decombe, F. J. Valdivia-Valero, G. Dantelle, G. Leménager, T. Gacoin, G. Colas des Francs, S. Huant, and J. Fick, "Luminescent nanoparticle trapping with far-field optical fiber-tip tweezers," Nanoscale **8**(9), 5334–5342 (2016).
21. G. Leménager, K. Lahlil, T. Gacoin, G. C. des Francs, and J. Fick, "Optical fiber tip tweezers, a complementary approach for nanoparticle trapping," J. Nanophotonics **13**(01), 1–9 (2018).
22. A. Kumar, J. Kim, K. Lahlil, G. Julie, S. Nic Chormaic, J. Kim, T. Gacoin, and J. Fick, "Optical trapping and orientation-resolved spectroscopy of europium-doped nanorods," JPhys Photonics **2**(2), 025007 (2020).
23. E. R. Lyons and G. J. Sonek, "Confinement and bistability in a tapered hemispherically lensed optical fiber trap," Appl. Phys. Lett. **66**(13), 1584–1586 (1995).
24. A. Asadollahbaik, S. Thiele, K. Weber, A. Kumar, J. Drozella, F. Sterl, A. M. Herkommer, H. Giessen, and J. Fick, "Highly efficient dual-fiber optical trapping with 3D printed diffractive fresnel lenses," ACS Photonics **7**(1), 88–97 (2020).
25. P. Haro-Gonzalez, B. Del Rosal, L. M. Maestro, E. M. Rodriguez, R. Naccache, J. Capobianco, K. Dholakia, J. G. Sole, and D. Jaque, "Optical trapping of $NaYF_4$: Er^{3+}, Yb^{3+} upconverting fluorescent nanoparticles," Nanoscale **5**(24), 12192–12199 (2013).
26. A. Jain, P. G. Fournier, V. Mendoza-Lavaniegos, P. Sengar, F. M. Guerra-Olvera, E. I niguez, T. G. Kretzschmar, G. A. Hirata, and P. Juárez, "Functionalized rare earth-doped nanoparticles for breast cancer nanodiagnostic using fluorescence and ct imaging," J. Nanobiotechnol. **16**(1), 26 (2018).
27. G. Leménager, M. Thiriet, F. Pourcin, K. Lahlil, F. Valdivia-Valero, G. C. des Francs, T. Gacoin, and J. Fick, "Size-dependent trapping behavior and optical emission study of $NaYF_4$ nanorods in optical fiber tip tweezers," Opt. Express **26**(24), 32156–32167 (2018).
28. S. K. Mondal, S. S. Pal, and P. Kapur, "Optical fiber nano-tip and 3D bottle beam as non-plasmonic optical tweezers," Opt. Express **20**(15), 16180–16185 (2012).
29. M. Woerdemann, C. Alpmann, M. Esseling, and C. Denz, "Advanced optical trapping by complex beam shaping," Laser Photonics Rev. **7**(6), 839–854 (2013).
30. K. Vairagi, R. A. Minz, S. Kaur, D. Kumbhakar, S. Paul, U. Tiwari, R. K. Sinha, J. Fick, and S. K. Mondal, "Deep seated negative axicon in selective optical fiber tip and collimated Bessel beam," IEEE Photonics Technol. Lett. **29**(10), 786–789 (2017).
31. J. Arlt and K. Dholakia, "Generation of high-order Bessel beams by use of an axicon," Opt. Commun. **177**(1-6), 297–301 (2000).
32. A. Aiello and G. S. Agarwal, "Wave-optics description of self-healing mechanism in Bessel beams," Opt. Lett. **39**(24), 6819–6822 (2014).
33. Z. Yang, X. Lin, H. Zhang, Y. Xu, L. Jin, Y. Zou, and X. Ma, "Research on the special bottle beam generated by asymmetric elliptical Gaussian beams through an axicon-lens system," Opt. Lasers Eng. **126**, 105899 (2020).

OSA CONTINUUM

34. S. K. Mondal, A. Mitra, N. Singh, S. Sarkar, and P. Kapur, "Optical fiber nanoprobe preparation for near-field optical microscopy by chemical etching under surface tension and capillary action," Opt. Express **17**(22), 19470–19475 (2009).
35. J.-B. Decombe, S. K. Mondal, D. Kumbhakar, S. S. Pal, and J. Fick, "Single and multiple microparticle trapping using non-Gaussian beams from optical fiber nanoantennas," IEEE J. Sel. Top. Quantum Electron. **21**(4), 247–252 (2015).
36. K. Berg-Sørensen and H. Flyvbjerg, "Power spectrum analysis for optical tweezers," Rev. Sci. Instrum. **75**(3), 594–612 (2004).
37. A. van der Horst and N. R. Forde, "Power spectral analysis for optical trap stiffness calibration from high-speed camera position detection with limited bandwidth," Opt. Express **18**(8), 7670–7677 (2010).
38. E. Florin, A. Pralle, E. Stelzer, and J. Hörber, "Photonic force microscope calibration by thermal noise analysis," Appl. Phys. A **66**(7), S75–S78 (1998).
39. A suitable alternative fiber is Nufern GF3.
40. S. K. Mondal, A. Mitra, N. Singh, F. Shi, and P. Kapur, "Ultrafine fiber tip etched in hydrophobic polymer coated tube for near-field scanning plasmonic probe," IEEE Photonics Technol. Lett. **23**(19), 1382–1384 (2011).
41. F. Wang, Y. Han, C. S. Lim, Y. Lu, J. Wang, J. Xu, H. Chen, C. Zhang, M. Hong, and X. Liu, "Simultaneous phase and size control of upconversion nanocrystals through lanthanide doping," Nature **463**(7284), 1061–1065 (2010).
42. X. Wang, J. Zhuang, Q. Peng, and Y. Li, "A general strategy for nanocrystal synthesis," Nature **437**(7055), 121–124 (2005).
43. G. Leménager, S. Tusseau-Nenez, M. Thiriet, P.-E. Coulon, K. Lahlil, E. Larquet, and T. Gacoin, "$NaYF_4$ microstructure, beyond their well-shaped morphology," Nanomaterials **9**(11), 1560 (2019).
44. G. Volpe and G. Volpe, "Simulation of a Brownian particle in an optical trap," Am. J. Phys. **81**(3), 224–230 (2013).
45. M. Tirado and J. G. de la Torre, "Translational friction coefficients of rigid, symmetric top macromolecules. application to circular cylinders," J. Chem. Phys. **71**(6), 2581–2587 (1979).